Thermal Behavior and Characterization of Poly[1,3-phenylenebis (methylene)adipamide]

Choichiro SHIMASAKI,* Hisashi SANAGI, Akira UNISHI, Hisakimi NOTOYA, Eiichi TSUKURIMICHI, and Toshiaki YOSHIMURA
Faculty of Engineering, Toyama University, Gofuku, Toyama 930
(Received October 9, 1990)

Thermal degradation of poly[1,3-phenylenebis(methylene) adipamide] (MXD-6) was investigated by DTA-TG, FT-IR, TG-GC/MS, and mass spectroscopy. The DTA-TG/DTG curve showed that the thermal decomposition of MXD-6 occurred in two stages. MXD-6 melted at about 235 °C and decomposed to the oligomer or monomer with a weight loss of about 40% in the temperature region from 330 to 400 °C during the first stage. A TG effluent gas was collected in a cold trap and then directly injected into a GC for separation, the MS for an unequivocal identification. The eleven effluent compounds from the thermal degradation of MXD-6 were identified. The main fragmentation mechanism by electron impact for MXD-6 consisted of two processes: simple cleavage and a rearrangement reaction. The activation energy of the thermal decomposition was estimated to be 230 during the first stage and 150 kJ mol^{-1} during the second stage. From the value of the activation energy in each stage, the kinetic data for MXD-6 was elucidated.

The structual characterization of Poly[1,3-phenylenebis(methylene)adipamide] (MXD-6) has attracted much attention recently, since this material is an important member of a family of polyamides. This family has potential for both thermohardening materials and important commercial polymers. Its, thus, thermal decomposition mechanism is of practical and theoretical relevance. Serveral thermal decomposition products have been identified in a flash pyrolysis GC study of several nylons.[1] Since the advent of modern direct pyrolysis mass spectrometry techniques, the thermal degradation of polyamides has been the subject of several publications.[2] The polymer (**I**) of isophthalic acid and hexamethylenediamine is amorphous and has relatively low melting and heat destortion temperatures.[3] MDX-6 shows the effects caused by a reversal of the position of the carbonyl groups relative to the amide nitrogen, in comparison with **I**.[4] It was of interest to investigate the thermal properties of MXD-6 in question be applying both TG and DTA techniques. Also, since little is known about the thermal behavior, such as the TG-GC/Mass, detailed degradation studies were performed; the results are discussed.

Experimental

Materials. MXD-6 polyamide (**II**) was produced by Mitsubishi Gasukagaku Co., Ltd. The following samples were selected for the present work. Sample (**IIa**): The powdered sample was prepared by cutting the rod of **II** with a saw. Sample (**IIb**): A powdered sample was prepared by refluxing in dimethylformamide solvent, then evaporating to dryness under reduced pressure. Sample (**IIc**): A colloidal solution after refluxing of **IIb** was filtered, washed with chloroform, and dried in air. Sample (**IId**): Powdered sample was prepared by sawing a rod of **II** with an electromobile high-speed saw. The elemental analyses of each sample are summarized, together with the calculated value of the monomer of **II** in Table 1.

All other chemicals were of the highest commercially available purity and were used without further purification, unless otherwise stated.

Thermal Analysis. Thermal analyses were performed using a Rigaku Denki thermogravimetry-differential thermal analysis (TG-DTA) and a differential scanning calorimetry (DSC) apparatus in air at various heating rates. Calcinated alumina was used as the reference material. TG-TRAP-GC/MS was carried out with a Shimadzu combined system in stationary helium gas at a heating rate of 10 °C min^{-1}. Separation and identification of the pyrolysis products were carried out by using a gas chromatograph coupled with a mass selective detector. A Shimadzu gas chromatograph, containing a capillary column of porous polymer beads of poly[oxy(2,6-diphenyl-1,4-phenylene)] (TENAX GC), coupled with a mass selective detector was used. The injector and detector temperatures were maintained at 230 and 250 °C.

Spectroscopic Measurements. A double-focussing JEOL-JMS-D300 mass spectrometer, equipped with the standard EI was used to obtain the mass spectra. The instrument was scanned from m/z 20 to 1000 at a scan rate of 10 s/decade; perfluorokerosene (PFK) was used for the computor calibration. The ion source was maintained at 200 °C. Polymers were pyrolyzed directly in the ion source using direct probes, heated from 20 to 350 °C at a heating rate of 10 °C min^{-1}.

Table 1. Elemental Analysis of **II**

Sample	N/%	C/%	H/%
IIa	10.58	64.11	7.50
IIb	10.98	60.80	7.19
IIc	10.94	63.89	7.49
IId	11.07	64.99	7.46
Monomer[a)]	10.60	63.61	7.63

a)

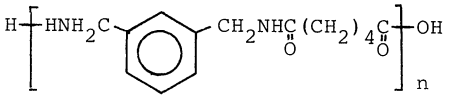

Poly(m-xylylene adipamide)
n=1: Monomer

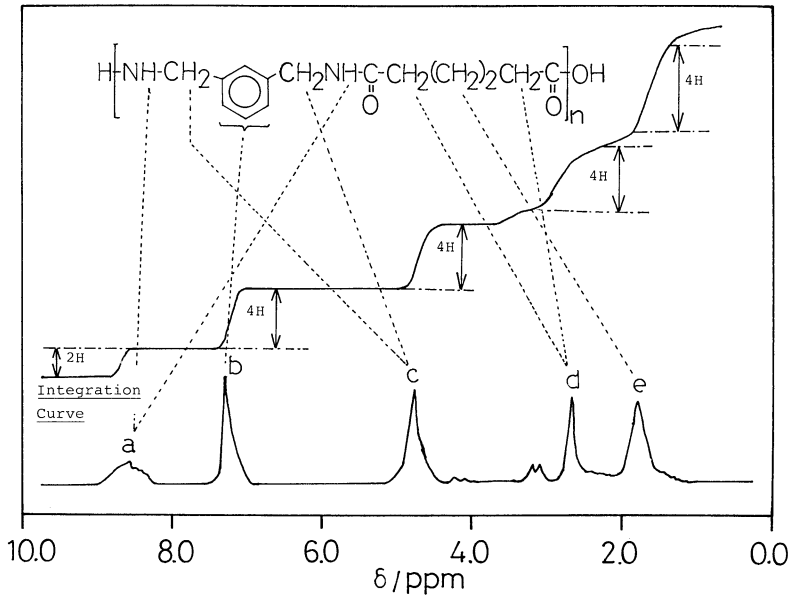

Fig. 1. ^{1}H NMR spectrum of **II**.

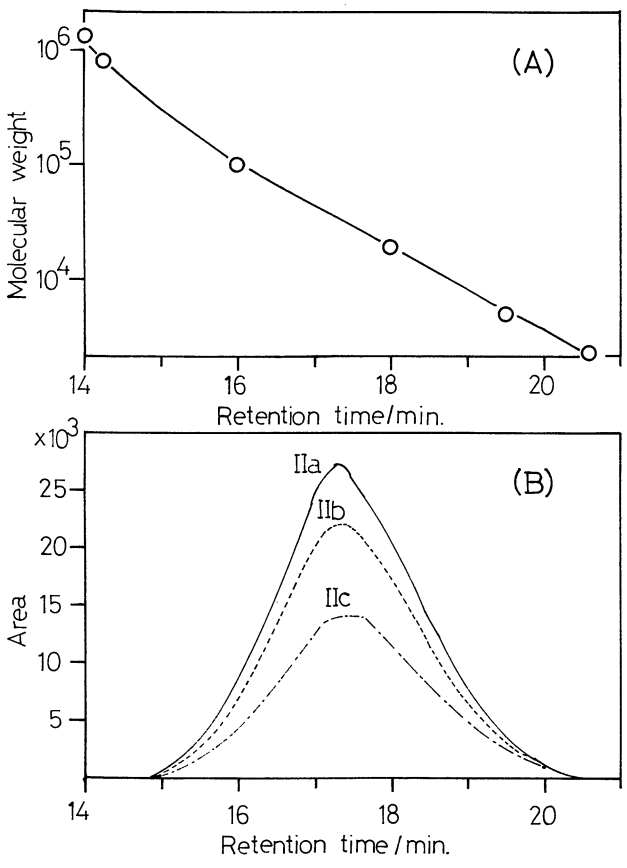

Fig. 2. GPC measurements for **II**. (A) Calibration curves of molecular weight with poly(methyl methacryrate). (B) Distribution curves of molecular weight for **II**.

Table 2. Molecular Weight for **II** by the GPC Measurement

Sample	MW[a]	MN[b]	MZ[c]	MW/MN
IIa	39250	19397	75589	2.02
IIb	38801	18934	74584	2.05
IIc	36525	16920	71459	2.16

a) MW=Weight-average molecular weight. b) MN=Number average molecular weight. c) MW=Z average molecular weight.

The IR spectrum was recorded using a JASCO FT-IR-3 type for both powder and thin films. The ^{1}H and ^{13}C NMR spectra were measured in trifluoroacetic acid using a JNM-FX-90-FT-NMR instrument. TMS was used as a reference. For the NMR spectrometric detection and identification of **II**, a solution containing trace amounts of insoluble materials was filtered with a molecular sieve. The ^{1}H NMR spectra given in Fig. 1 shows that **II** contains the constituent functional groups. The steps in the integration curve in Fig. 1 provide the ratios for the different kinds of protons in the molecule. These can be compared with the proton count obtained from the off-resonance decoupled ^{13}C spectrum.

GPC Analysis. A Waters 6000A apparatus equipped with a gel permeation chromatography (GPC) HFIP-80M column was used. A differential refractometer was used as the detector. Analyses were performed at 40 °C in 1,1,1,3,3,3,-hexafluoro-2-propanol (HFIP) as the eluent at a flow rate of 0.5 ml min^{-1}. The working curve was obtained by a calibration with poly(methyl methacrylate) of known molecular weight, as shown in Fig. 2(A). Also, Fig. 2(B) shows the relationship between the area and the retention time with the GPC measurements. The experimental data of each molecular weight for **II** are summarized in Table 2.

Results and Discussion

Thermal Analysis. The TG-DTA curves relative to **IIa** and **IId** are shown in Fig. 3. Figure 3 shows that a melting points are present in the DTA curves for **IIa** and **IId** at 234.6 and 235.5 °C, respectively. From the measurement of DSC, the heat of fusion for **II** was estimated to be about 42 J g^{-1}. The TG-DTA curves of **IIa**, **IIb**, and **IIc** are practically coincident, and the maximum volatilization rate was observed at about 370 and 470 °C. It is borne by changes in the IR spectra both before and after the heating of **II**. Figure 4 shows the change of the IR spectra between room temperature and 400 °C. For the IR spectrum of **II**, the absorption band between 1000 and 1200 cm^{-1} is assigned to the C–N stretching vibration. This absorption grew weaker at 400 °C. At about 2400 cm^{-1} the absorption band attributed to the N–H stretching vibration grew strong, showing that the cleavage of C–N proceeded. Upon further heating, the less-stable aliphatic groups were preferentially decomposed through the homolytic cleavages of the C–C, C–H, C–N, and N–H bonds. Since the thermal degradation in the present work was carried out in a static air medium, it can be said that atmospheric oxygen is consumed before combustion is completed, and that the remainder decomposes afterwards in an inert medium. The last exotherm on the DTA curve of **IId** represents a crosslinking and aromatization of the char in an inert medium.

To investigate the thermal decomposition processes which cause the DTA and the TG curves over the range from 200 to 500 °C for **II**, TG-TRAP-GC/MS was carried out in stationary He. In many cases the TG effluent gas was comprised of various components. The identification of less-abundant components became increasing difficult. Another approach is to collect the pyrolysis products and then to analyze this collected material by GC. This method has been applied to the analysis of thermal degradation products.[5] Figure 5 shows a mass chromatogram of the liberated decomposition products of **II** with a tandem thermogravimetric analyzer–gas chromatograph–mass spectrometer system. The thermally degraded products of **II** consist of about eleven components. These components were identified by measuring the mass spectrum of the liberated gas from

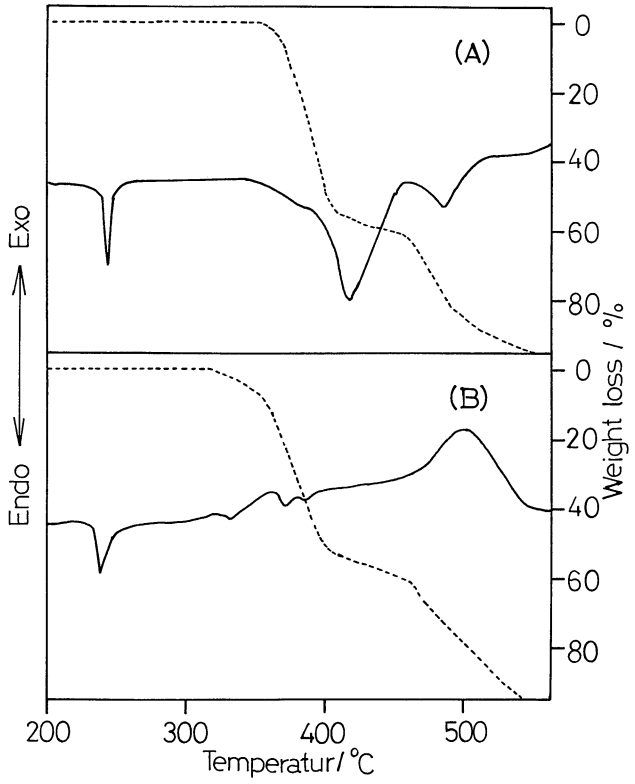

Fig. 3. Effect of pretreatment method on the DTA curves of **II**. (A) **IIa**: Powdered sample prepared by sawing rod of **II** with saw. (B) **IId**: Powdered sample prepared by sawing rod of **II** with the electromobile high speed saw.

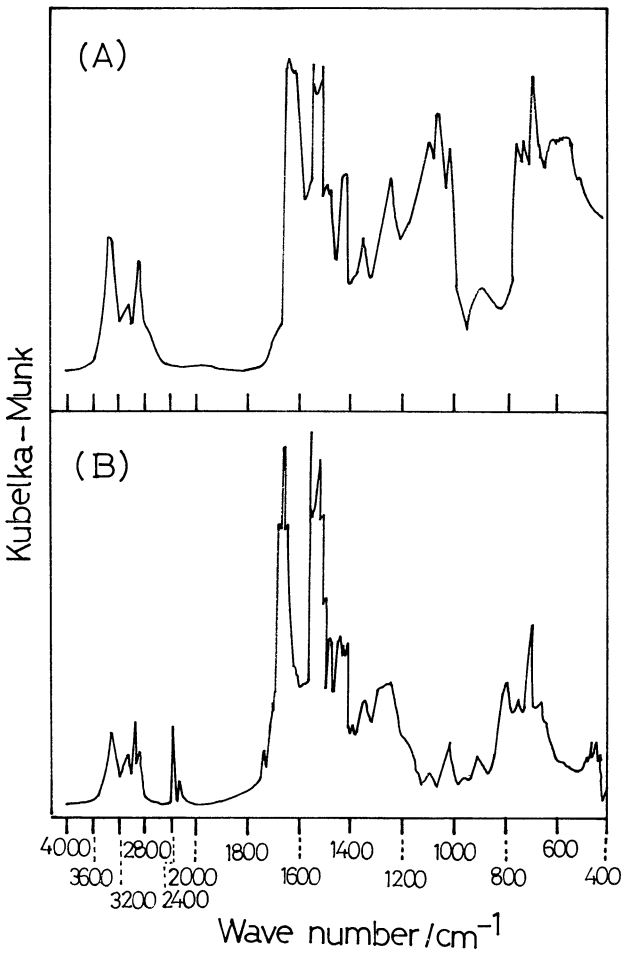

Fig. 4. Effect of heating temperature on the FT-IR spectra of **II**. (A) Sample at the room temperature. (B) Sample heated at 400 °C.

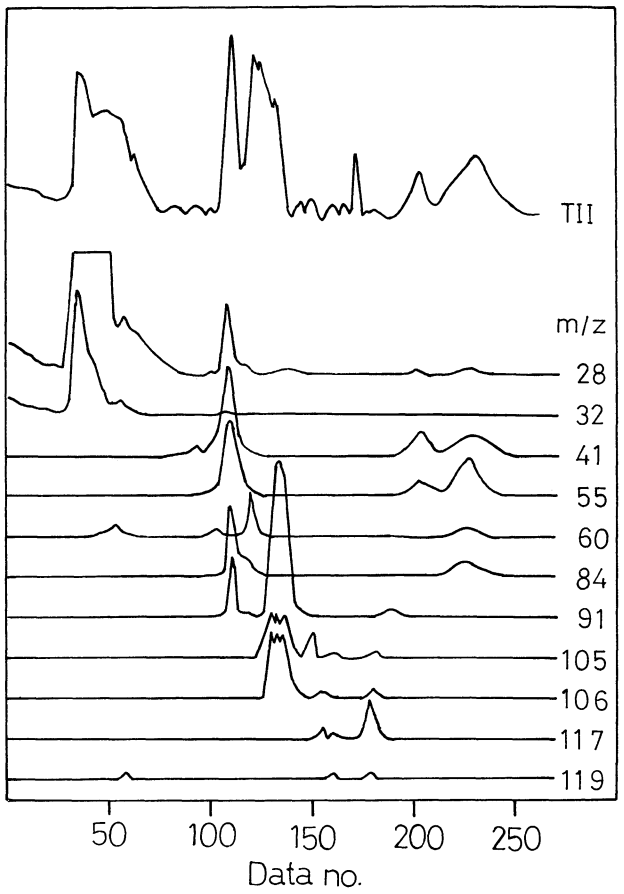

Fig. 5. Mass chromatogram of the decomposition products of **II** with TG-TRAP-GC/MS. TII=Total Ion Intensity.

the principal portion of the weight loss on the TG curve between 300 and 500 °C. The peaks at *m/z* 28 and 32 due to N_2 (or CO) and O_2 were the most intense. The peak at *m/z* 119 due to $C_8H_9N^+$ was the apparent maximum mass number in the liberated decomposition products of **II**. Other thermally degraded products of **II** consists of a complex mixture of seven components: $(C_7H_7NH_2)^+$ *m/z* 106→$(C_7H_7NH)^+$ *m/z* 105; $(C_7H_7)^+$(Tropylium ion) *m/z* 91; $(C_4H_4CO)^+$ *m/z* 84; $(C_4H_7)^+$ *m/z* 55→$(C_3H_5)^+$ *m/z* 41→$(C_2H_4)^+$ *m/z* 28. These components were identified by measuring the mass chromatograms of the decomposition products of **II** (Fig. 5). This result shows that the thermal degradation of **II** takes place through two alternative pathways. The first one dominates below 300 °C and involves dehydration, rearrangement, evolution of carbon monooxide and carbon dioxide, and the formation of carbonaceous residue. The second one, which starts at about 400 °C and overshadows the first one at higher temperatures, involves cleavages of the *m*-phenylenebis(methyleneimino) units by intramolecular rearrangements and the formation of a tar mixture and some randomly linked low molecular weight aliphatic derivatives, which then evaporate.

Mass Spectrum. The thermal decomposition process may be directly predictable from the corresponding mass spectrum. The main mass spectral data of low- and high-resolution is shown in Table 3. This table tabulates *m/z*, its corresponding elemental composition, and the probable molecular structure of each of the identified components. The ion of largest

Table 3. Mass Spectral Data for **II**

m/z[a]	Relative intensity[b]	Sigma/%[c]	Observed molecular weight	U.S.[e]	Probable ion composition
55	701.1	8.05	55.0188 (55.0183)[d]	2.5	C_3H_3O
			55.0578 (55.0546)	1.5	C_4H_7
56	276.9	3.18	56.0269 (56.0261)	2.0	C_3H_4O
			56.0631 (56.0624)	1.0	C_4H_8
77	23.1	0.26	77.0349 (77.0390)	4.5	C_6H_5
78	12.9	0.14	78.0485 (78.0468)	4.0	C_6H_6
79	46.1	0.52	79.0514 (79.0546)	3.5	C_6H_7
82	104.8	1.20	82.0637 (82.0654)	2.5	C_5H_8N
84	419.3	4.81	84.0560 (84.0573)	2.0	C_5H_8O
91	140.2	1.61	91.0510 (91.0546)	4.5	C_7H_7
104	262.7	3.01	104.0636 (104.0624)	5.0	C_8H_8
105	166.1	1.98	105.0636 (105.0576)	5.0	C_7H_7N
106	469.5	5.39	106.0659 (106.0654)	4.5	C_7H_8N
118	274.4	3.15	118.0712 (118.0654)	5.5	C_8H_8N
119	1000.0	11.48	119.0733 (119.0732)	5.0	C_8H_9N
120	420.7	4.83	120.0846 (120.0810)	4.5	$C_8H_{10}N$
133	173.4	1.99	133.0695 (133.0762)	5.5	$C_8H_9N_2$
134	133.5	1.53	134.0854 (134.0840)	5.0	$C_8H_{10}N_2$
135	193.0	2.21	135.0930 (135.0918)	4.5	$C_8H_{11}N_2$
146	92.5	1.06	146.0587 (146.0603)	6.5	C_9H_8NO
161	134.2	1.54	161.0676 (161.0711)	6.5	$C_9H_9N_2O$
189	129.7	1.48	189.1079 (189.1023)	6.5	$C_{11}H_{13}N_2O$
218	197.2	2.26	218.1399 (218.1413)	6.0	$C_{13}H_{18}N_2O$
246	174.8	2.00	246.1408 (246.1362)	7.0	$C_{14}H_{18}N_2O_2$

a) The $(M-H_2O)^+$ of monomer is underlined. b) Relative intensity referred to base peak of spectrum as 1000. c) Peak hights expressed in per cent of total ionization. d) Calculated values. e) U.S.=Degree of unsaturation.

intensity in the spectrum was selected in order to obtain the relative intensity of the raw peak height of the fragment ion. The intensity of this ion peak is called the base peak intensity. The base peak appeared at m/z 119 due to $C_8H_9N^+$. The spectrum also indicates that the peak of the maximum mass number is the $(M-H_2O)^+$ of monomer. The observed mass spectrum is an averaged recording of the results of a host of fragmentation events, most of which represent only the results of a relatively few successive fragmentations to a given moiety. A compound of **II** after ionization of the $(M-H_2O)^+$ can produce cleavages to produce fragment of m/z 100, 119, 134, 161, 189, 218, and 246, as shown in Fig. 6. Simple cleavages, such as fragment ion 1, 2, 5, and 6, as indicated by the wave line, of an even-electron ion produce another even-electron ion and a neutral olefin or other neutral particles. In fragment ion 3,4, and 7, however, the cleavage is due to the well-known McLafferty rearrangement process.

Kinetic Analysis of the Thermal Decomposition. The kinetic discussion was carried out in terms of the thermal analysis according to the Ozawa method.[6] The sample was lightly packed with the aid of a special holder into an aluminum pan. Thermal decomposition was studied at heating rates of 1.0, 3.0, 5.0, 7.0, and 10.0 °C min^{-1}. Figure 7 shows the TG curves for **II**, as determined at different heating rates. According to the Ozawa theory, the weight loss (θ) at a constant heating rate can be expressed by

$$\theta = \Delta E/aR \cdot P(\Delta E/RT), \quad (1)$$

where ΔE is the activation energy; a, the heating rate, and R, the gas constant. Also, in the case $60 > \Delta E/RT > 20$,

$$\log P(\Delta E/RT) = -\log a - 0.456\Delta E/RT. \quad (2)$$

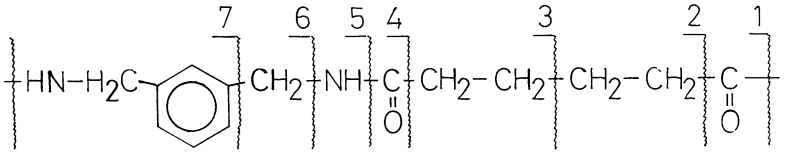

Fragment ions

1. $C_{14}H_{18}N_2O_2^+$ m/z 246
2. $C_{13}H_{18}N_2O^+$ m/z 218
3. $C_{11}H_{13}N_2O^+$ m/z 189
4. $C_9H_9N_2O^+$ m/z 161
5. $C_8H_{10}N_2^+$ m/z 134
6. $C_8H_9N^+$ m/z 119
7. $C_7H_8N^+$ m/z 100

Fig. 6. Main fragment ions by the electron impact for **II**.

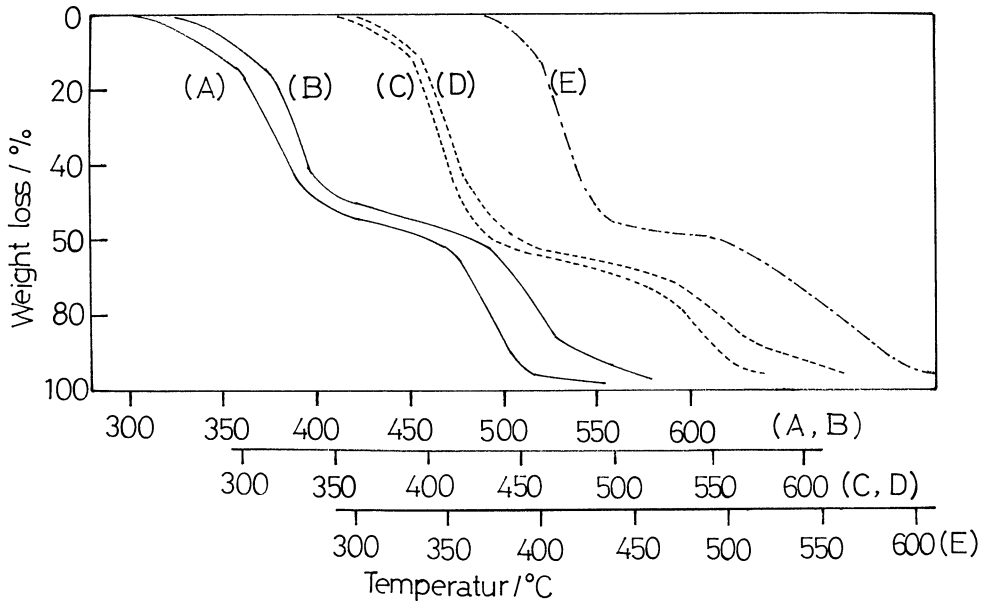

Fig. 7. TG curves for **II** at various heating rates. (A) 1.0, (B) 3.0, (C) 5.0, (D) 7.0, (E) 10.0 °C min^{-1}.

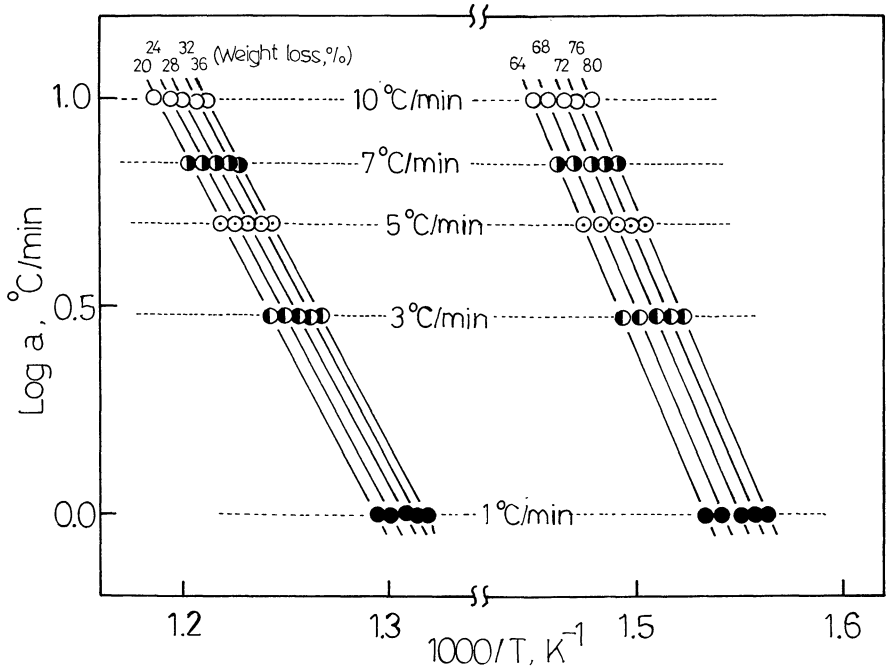

Fig. 8. Plots of logarithms of heating rate versus the reciprocal of absolute temperature for the given conversation of pyrolysis of **II**.

Table 4. Activation Energy for the Thermal Decomposition Process of **II**

Weight loss/%[a]	ΔE/kJ mol^{-1}[b]	r[c]	Process[d]
10	139	0.959	
20	188	0.987	
30	196 (203)	0.970	First stage
40	226	0.980	
50	399	0.941	
60	921	0.596	Flat portion
70	200	0.979	
80	146 (168)	0.988	Second stage
90	113	0.943	

a) Weight loss on the TG curve. b) Calculated by Ozawa's method. The values in parenthese were graphically calculated. c) Linear correlation coefficient. d) Each process on the TG curve.

Table 5. Kinetic Data for the Thermal Decomposition Process on the TG Curve for **II**

Thermal decomposition process	Reaction order	Frequency factor
First stage	0.974	0.88×10^{10}
Second stage	0.531	0.12×10^{9}

From plots of the logarithms of the heating rate versus the reciprocal of the absolute temperature for the given residual weight, the activation energy was obtained by the slope of the straight lines. In Fig. 8 is shown Ozawa's plot of the logarithmic heating rate versus the reciprocal absolute temperature. Table 4 shows the values of the activation energy, which was calculated from each weight loss on the TG curves. The activation energies of the first and second stage average 230 and 150 kJ mol^{-1}, respectively. The former was due to the main thermal decomposition while the latter resulted in an oxidative reaction. For nylon, the activation energy was evaluated to be 155 kJ mol^{-1} in Inoue and Sumoto's paper,[7] in which the mechanism of the unzipping of the monomer from carboxyl ends was postulated. The difference between the result in the first stage of this paper and in Inoue et al. paper is dependent upon the complexity of the group attached to the carbonyl carbon atom. It is possible to estimate the reaction order and the frequecy factor in each stage of the thermal decomposition process for **II** by employing the values of activation energy and the direct search method. The results are summarized in Table 5. This thermal decomposition process for **II** obeys a first-order rate law during the first stage and 1/2 order during the second stage. In order to examine the kinetic data, the present authors compared the observed value of the reaction rate and the frequecy factor with the calculated value. The results given in Table 6 agree with the expectations.

We wish to thank Miss Misao Shinoda for the Mass spectra and Mr. Yoshiharu Yoneyama for NMR measurements.

Table 6. Applicability of the Equation of $dX/dt=A \exp(-E/RT)X^n/B$, $B=1.0\,^\circ C\,min^{-1}$

TG curve[a)]	Temperature/K	Partial fraction of residue weight X	dX/dT	
			Observed	Calculated
First stage	579	0.956	$0.3250\ 10^{-2}$	$0.2467\ 10^{-2}$
	609	0.849	$0.6330\ 10^{-2}$	$0.9107\ 10^{-2}$
	628	0.698	$0.1537\ 10^{-1}$	$0.1726\ 10^{-1}$
	643	0.398	$0.2303\ 10^{-1}$	$0.1858\ 10^{-1}$
	653	0.202	$0.1388\ 10^{-1}$	$0.1429\ 10^{-1}$
	672	0.031	$0.4000\ 10^{-3}$	$0.4746\ 10^{-2}$
Seond stage	688	1.000	$0.1650\ 10^{-2}$	$0.3680\ 10^{-2}$
	713	0.920	$0.4370\ 10^{-2}$	$0.8227\ 10^{-2}$
	731	0.799	$0.1237\ 10^{-1}$	$0.1353\ 10^{-1}$
	749	0.467	$0.2065\ 10^{-1}$	$0.1729\ 10^{-1}$
	768	0.133	$0.1330\ 10^{-1}$	$0.1475\ 10^{-1}$
	783	0.0001	$0.1810\ 10^{-2}$	$0.3817\ 10^{-3}$

a) Measured at heating rate of $1.0\,^\circ C\,min^{-1}$.

References

1) H. Ohtani, T. Nagaya, Y. Sugimura, and S. Tsuge, *J. Anal. Appl. Pyrolysis*, **4**, 117 (1982).

2) I. Luderwald and H. R. Kricherdorf, *Angew. Makromol. Chem.*, **56**, 173 (1976); I. Luderwald, F. Merz, and H. Rothe, *ibid.*, **67** 193 (1978); I. Luderwald and F. Merz, *ibid.*, **74**, 165 (1978); U. Bahr, I. Luderwald, R. Muller, and R. H. Shulten, *ibid.*, **120**, 163 (1984); R. H. Shulten and H. J. Dussel, *J. Anal. Appl. Pyrolysis*, **2**, 293 (1980); A. Ballistreli, D. Garozzo, M. Giuffrida, and G. Montaudo, *Macromolecules*, **20**, 2991 (1987).

3) F. G. Lum and E. F. Carlston, *Ind. Eng. Chem.*, **44**, 1595 (1952).

4) E. F. Carlston and F. G. Lum, *Ind. Eng. Chem.*, **49**, 1239 (1957).

5) E. A. Boettner, G. Ball, and B. Weiss, *J. Appl. Polym. Sci.*, **13**, 377 (1969); W. H. Hale, A. G. Farham, R. N. Johnson, and R. A. Clendiving, *J. Polym. Sci., Part A-1*, **5**, 2399 (1967); J. Chia, *Thermochim. Acta*, **1**, 231 (1970); J. Chiu, *Anal. Chem.*, **40**, 1516 (1968).

6) T. Ozawa, *Bull. Chem. Soc. Jpn.*, **38**, 1881 (1965); T. Ozawa, *J. Therm. Anal.*, **2**, 301 (1970).

7) R. Inoue and M. Sumoto, *Chem. High Polym.*, **11**, 169 (1954).